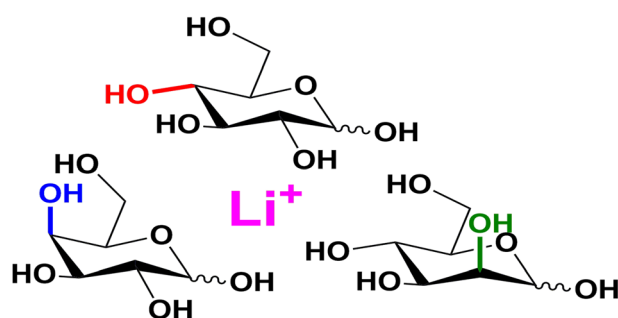**RESEARCH ARTICLE**

Fragmentation Pathways of Lithiated Hexose Monosaccharides

Maha T. Abutokaikah,[1] Joseph W. Frye,[1] John Tschampel,[2] Jordan M. Rabus,[1] Benjamin J. Bythell[1]

[1]Department of Chemistry and Biochemistry, University of Missouri, St. Louis, MO 63121, USA
[2]University City High School, 7401 Balson Ave, University City, MO 63130, USA

Abstract. We characterize the primary fragmentation reactions of three isomeric lithiated D-hexose sugars (glucose, galactose, and mannose) utilizing tandem mass spectrometry, regiospecific labeling, and theory. We provide evidence that these three isomers populate similar fragmentation pathways to produce the abundant cross-ring cleavage peaks ($^{0,2}A_1$ and $^{0,3}A_1$). These pathways are highly consistent with the prior literature (Hofmeister et al. J. Am. Chem. Soc. **113**, 5964–5970, 1991, Bythell et al. J. Am. Soc. Mass Spectrom. **28**, 688–703, 2017, Rabus et al. Phys. Chem. Chem. Phys. **19**, 25643–25652, 2017) and the present labeling data. However, the structure-specific energetics and rate-determining steps of these reactions differ as a function of precursor sugar and anomeric configuration. The lowest energy water loss pathways involve loss of the anomeric oxygen to furnish B_1 ions. For glucose and galactose, the lithiated α-anomers generate ketone structures at C2 in a concerted reaction involving a 1,2-migration of the C2-H to the anomeric carbon (C1). In contrast, the β-anomers are predicted to form 1,3-anhydroglucose/galactose B_1 ion structures. Initiation of the water loss reactions from each anomeric configuration requires distinct reactive conformers, resulting in different product ion structures. Inversion of the stereochemistry at C2 has marked consequences. Both lithiated mannose forms expel water to form 1,2-anhydromannose B_1 ions with the newly formed epoxide group above the ring. Additionally, provided water loss is not instantaneous, the α-anomer can also isomerize to generate a ketone structure at C2 in a concerted reaction involving a 1,2-migration of the C2-H to C1. This product is indistinguishable to that from α-glucose. The energetics and interplay of these pathways are discussed.

Keywords: Mass spectrometry, Collision-induced dissociation, Ion structure, Labeling, Metal ions, Density functional theory, Glycans

---

Electronic supplementary material The online version of this article (https://doi.org/10.1007/s13361-018-1973-3) contains supplementary material, which is available to authorized users.

Correspondence to: Benjamin Bythell; *e-mail:* bythellb@umsl.edu

Introduction

Carbohydrates play vital roles in biology but are often difficult to identify confidently from these samples [1–5]. One of the most challenging aspects of biological carbohydrate research is the need to distinguish between multiple isomeric structures [6–17]. This has led to a proliferation of mass spectrometry-based methods aimed at mitigating this

problem [3, 6, 8–12, 18–30]. Complex polysaccharide carbohydrates are formed from simple monosaccharide units in glycosylation reactions. Hexose ($C_6H_{12}O_6$) monosaccharides are the main building blocks of complex carbohydrates [5]. In the present article, we investigate the gas-phase fragmentation chemistry of three hexopyranose monosaccharides common in living systems: glucose, galactose, and mannose (Figure 1). Lithium cationization is utilized. These analytes differ only in the stereochemistry of individual hydroxyl groups. However, these simple stereochemical variations can have a profound impact on the chemistry in biological systems [31] and the gas phase.

In the present article, we utilize tandem mass spectrometry (MS/MS) [32] and regiospecific isotopic labeling [1–3, 16, 21, 23, 24, 33, 34], coupled with theory [1, 2, 34, 35], to elucidate the characteristic fragmentation chemistry of lithiated monosaccharide analytes. The present manuscript is a follow-up to our [1, 2] and others' [34, 35] recent work on sodiated carbohydrate analytes (specifically requested by reviewers of the earlier paper). While there is certainly a wealth of relevant experimental work on lithiated carbohydrates (for example, [3, 12, 20, 25, 33]) and their fragmentation, there is little/no theoretical data on the specific fragmentation chemistry of these analytes [35, 36]. An analogous situation exists for theoretical data; a substantial number of studies on neutral carbohydrate geometries [37–40], but data on lithiated forms is lacking. In the present article, we investigate the primary, structurally useful, fragmentation pathways of lithiated glucose, galactose, and mannose: water loss (primarily B_1 ion formation) and the cross-ring cleavage reactions producing the $^{0,2}A_1$ and $^{0,3}A_1$ ions. We provide evidence for the key gas-phase structures, mechanisms, and energetics underlying these processes.

Experimental

The experimental work was done using an electrospray ionization MaXis plus quadrupole time-of-flight mass spectrometer
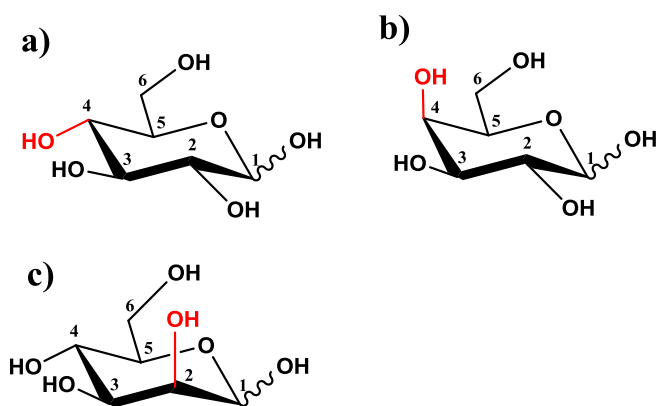

Figure 1. The different monosaccharide systems in this study. (a) Glucose. (b) Galactose. (c) Mannose. The anomeric center (carbon 1) configuration exists as a mixture of the axial (α) and equatorial (β) forms

(Bruker, Billerica, MA). The analytes were diluted to ~ 5 μM with acetonitrile/water/lithium chloride (50/50/0.1%) and then sprayed at a flow rate of 3 μl min^{-1}. Nitrogen was used as both nebulizing and drying gas. The lithiated analytes were selected using the quadrupole followed by activation by collision in the collision cell containing nitrogen. The resulting product ions and remaining precursor ions were dispersed by the time-of-flight mass analyzer. Data was collected as a function of collision energy. Exchange of the analyte hydroxyl protons for deuterons was achieved by dissolving the analytes in deuterium oxide (D_2O) for 10 min at room temperature, prior to further dilution in acetonitrile/D_2O/LiCl (50/50/0.1%) to a final concentration of ~ 5 μM [3]. Deuterium oxide was purchased from Cambridge Isotopes Laboratories, Inc. (Tewksbury, MA). Lithium chloride, HPLC-grade acetonitrile, and H_2O were purchased from Sigma-Aldrich (St. Louis, MO). regioselectively isotopically labeled monosaccharides were purchased from Cambridge Isotopes Laboratories, Inc. (Tewksbury, MA).

Theoretical Methods

Density functional calculations of minima, transition states, product ions, and neutrals were performed with the Gaussian 09 suite of programs [41] at the M06-2X/6-31+G(d,p) level of theory [42, 43]. Multiple conformers of each site of lithiation were examined for each system by scanning the potential energy surface. An initial pool of seed structures was generated using the molecular dynamics engine Fafoom [39, 40] via a genetic algorithm utilizing the MMFF94 force field [44–48]. These structures were sorted based on ring configuration and energy. Once a starting pool has been formed, the genetic algorithm begins with new trial structures generated based on components (i.e., torsion angles and ring configuration) of previous candidates/results. These trials are also subjected to geometry optimization and added to the candidate pool. The neutral structures were geometry optimized at the M06-2X/6-31G(d) level of theory in the Gaussian 09 suite of programs [41]. Following removal of degenerate structures, the optimized neutral candidate structures for each system were then lithiated utilizing a coordinate sensitive script. This process was repeated for all potential sites of lithium attachment. The resulting structures were optimized at the M06-2X/6-31+G(d,p) level of theory. Results of these calculations were then inspected. These structures were ranked based on electronic energy after which the lowest energy, non-degenerate structures were selected for vibrational analysis. Having characterized the low energy minima, multiple transition structures (TSs) were sought. Minima were checked by vibrational analysis (all real frequencies) and TSs were also examined in this manner (one imaginary frequency). The reaction pathway through each particular, energetically competitive TS was determined by intrinsic reaction coordinate (IRC) calculations with up to 18 steps in each direction. The terminating points of these calculations (one on product side, one on reactant side) were then optimized further to determine the exact minima

connected by each specific transition structure. Estimates of the lithium affinities of the leaving groups were determined as the difference between the zero-point energy-corrected M06-2X/6-31+G(d,p) total electronic energies (0 K) of the lithiated and neutral form plus Li^+ at infinite separation.

Results and Discussion

Experimental Findings

Lithiated glucose, galactose, and mannose analytes, $[C_6H_{12}O_6+{}^7Li]^+$, populate similar fragmentation pathways (Figure 2; for nomenclature, see Figure S1 [49]). They all produce a water loss peak at m/z 169 which is consistent with the literature on metal-cationized carbohydrate ions [1–3, 33, 34, 50, 51]. Lithiated analytes also produce peaks resulting from cross-ring cleavages. Unlike recent work from Chen et al. on sodiated glucose analytes [35], we observe two cross-ring cleavage peaks. Our accurate mass and labeling data supports assignments of $^{0,2}A_1$, $[C_4H_8O_4+{}^7Li]^+$ at m/z 127 and $^{0,3}A_1$, $[C_3H_6O_3+{}^7Li]^+$ at m/z 97 in all cases. The key difference between the three analyte populations is manifested in relatively small changes in the relative critical energy required to initiate fragmentation. The lithiated glucose and galactose

epimers fragment at lower collision energies than the mannose forms (Figure 2, Figure S2). In addition, the relative abundance of the peaks vary between the systems supporting either differing product dimer-constituents [1, 2] or energetics in each case.

Experimentally, the most facile, useful, reactions for $[glucose+{}^7Li]^+$ are water loss from the anomeric center (B_1, m/z 169) and a low abundance cross-ring cleavage $^{0,2}A_1$ peak. This is followed by another cross-ring cleavage peak, $^{0,3}A_1$, then consecutive losses of water molecules from the $^{0,2}A_1$ ion (m/z 109 and 91, Figure 2a, m/z 111 and 91, Figure S2a). We note that direct loss of Li^+ also occurs, but this is of no structural benefit.

The lithiated galactose analytes require a similar degree of activation for fragmentation to be experimentally observed. Both the degree of fragmentation as a function of collision energy (reduced relative to glucose) and the nature of the primary fragments differ. For $[galactose+{}^7Li]^+$, the primary fragments are $^{0,3}A_1$ and water loss (B_1) from the anomeric center (Figure 2b, Figure S2b), followed by the $^{0,2}A_1$ peak at increased collision energies. Similar to the glucose data, the $^{0,3}A_1$ peak is more prevalent than the $^{0,2}A_1$ peak at higher collision energies (Figures S3 and S4). Lithiated mannose is the least readily fragmented analyte experimentally (Figure 2c, Figure S2c). Similar to glucose, $[mannose+Li]^+$ produces both
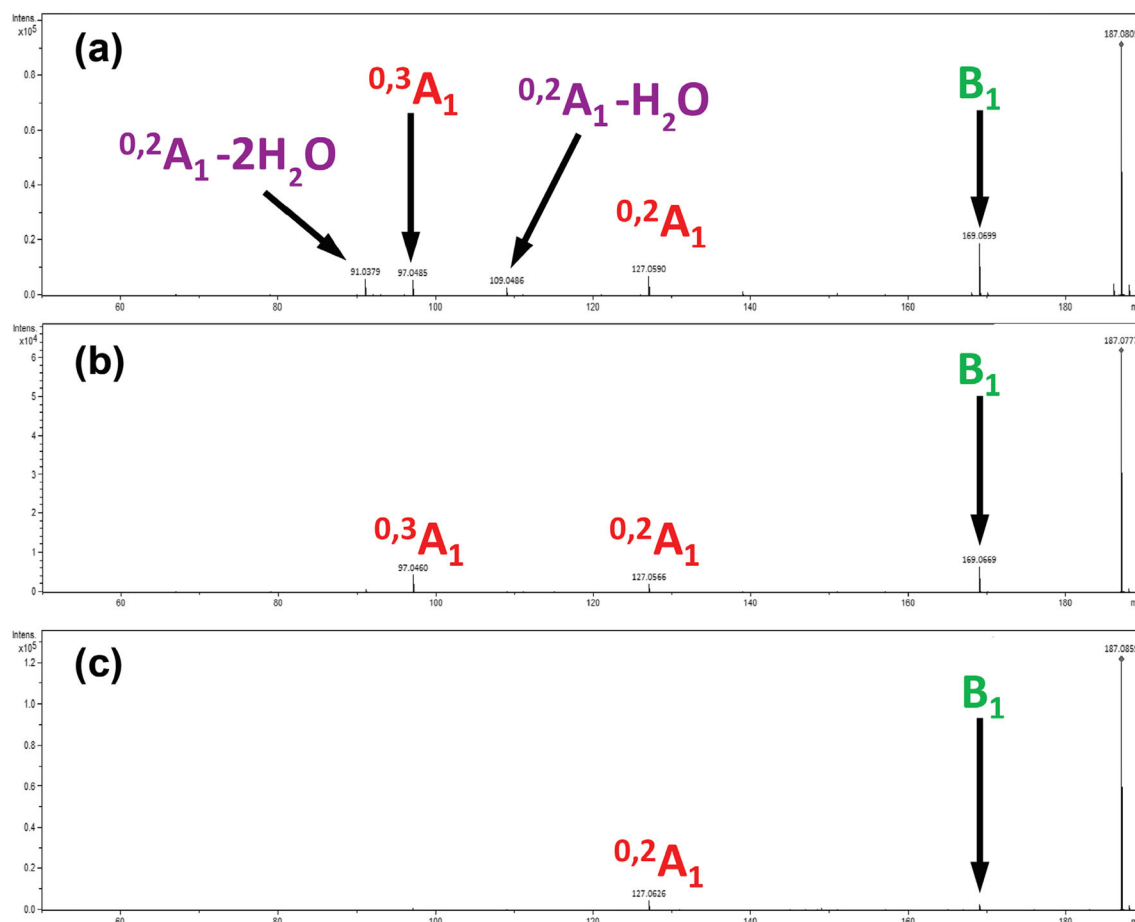

Figure 2. Example MS/MS spectra ($E_{collisions, lab}$ = 15 eV) of the isomeric lithium-cationized analytes. (a) Glucose. (b) Galactose. (c) Mannose

the water loss (B_1) and the $^{0,2}A_1$, $[C_4H_8O_4+Li]^+$ peaks. The $^{0,3}A_1$ ions are increasingly prevalent at higher collision energies (≥ 20 eV). However, unlike for the glucose and galactose congeners, the $^{0,2}A_1$ ions are most prominent at higher collision energies (Figure S5). In addition, myriad consecutive fragmentation processes are also possible (water losses, $C_2H_4O_2$ losses, etc.) at higher collision energies along with a substantial decrease in detectable ion signal resulting from loss of Li^+ and/or inability to efficiently capture the low m/z products. This general finding though not the exact product distribution also holds for the other monosaccharide analytes.

To distinguish the carbons and the hydrogen atoms contributing to fragment losses, we performed hydrogen-deuterium exchange of the hydroxyl protons forming $[C_6H_7D_5O_6+{}^7Li]^+$ precursor ions. These analytes were then subjected to collisional activation (Figure S2). Additional analyses of regiospecifically labeled (^{13}C, ^2D) forms of our analytes were also performed. The key findings are the following: (1) support for the $^{0,2}A_1$ and $^{0,3}A_1$ peak assignments over the isomeric X_0 ion possibilities (Tables S1–S3, Figure S1) and (2) that losses are of D_2O and not DOH to furnish the B_1 ions at m/z 172, i.e., no loss of C-alpha protons. This is entirely consistent with the prior literature [1–3, 33]. Data is provided in Figure S2 and Tables S1–S3 for the interested reader.

Energetics of Lithiated Minima

The lowest energy structures of glucose, galactose, and mannose are shown in Figure 3 and Figure S6. Our calculations indicate that the global minima of lithiated glucose are skew conformations ($^OS_2$) [52] in which the Li^+ is coordinated to the C3 and C6 hydroxyl oxygens (Figure 3a, Figure S6a). This contradicts the earlier claims of Ni and co-workers who did not locate any skew conformations [34]. The GM structures advocated by those authors have fewer oxygens coordinating the lithium cation and are 6.9 (α) and 17.7 (β) kJ mol^{-1} less energetically favorable based on our calculations. Skew conformations appear to be characteristic of lithiated systems as these same authors found them to be less competitive for sodiated glucose congeners [35]. Alternate low-energy families of lithiated glucose structures formed are chair conformations ($^1C_4$ and $^4C_1$) requiring at least 16 and 17 kJ mol^{-1} to populate (Figure S7). In contrast, the lowest energy conformation of the lithiated β-galactose anomer is a chair structure (Figure 3b). The [α-galactose+Li]$^+$ analytes are also predicted to form chair conformations (Figure S6b) as are both mannose anomeric forms (Figure 3c, Figure S6c).

Water Loss Pathways and B₁ Ion Formation

The water loss is initiated by proton transfer from one of the hydroxyl groups rather than a C_α proton (Scheme 1, Figure 4). Additional experimental evidence for this proposal is provided by our deuterated hydroxyl MS/MS experiments; loss of D_2O to produce the m/z 172 peak holds across all analytes examined in the present study (Figure S2). Our theoretical data predict that the lowest energy pathways to loss of water all include the
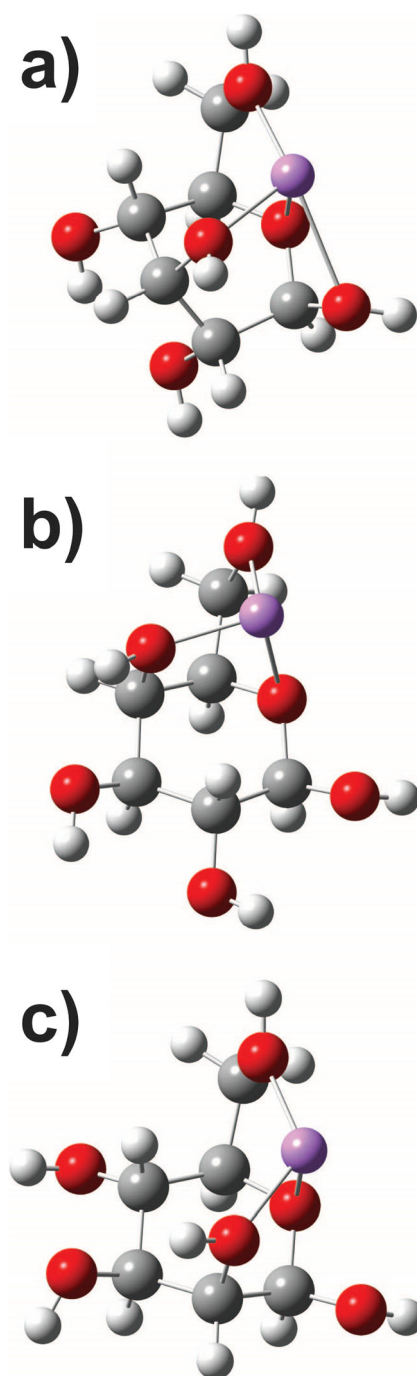

Figure 3. Global minima of the isomeric lithium-cationized analytes. (**a**) β-Glucose. (**b**) β-Galactose. (**c**) β-Mannose. β-Glucose adopts a skew conformation ($^OS_2$) while the galactose and mannose preferentially adopt chair conformations

anomeric oxygen. However, the exact structural specifics of this reaction are predicted to vary as a function of analyte type and anomeric configuration (Scheme 1, Scheme S1, Figure 4, Tables 1, 2, and 3, Tables S1–S3).

For all α-anomers, the water loss reaction is initiated by proton transfer to the anomeric hydroxyl group from the C2 hydroxyl (Scheme 1). For the glucose and galactose forms (Scheme 1a, Figure 1a, b), this proton transfer is
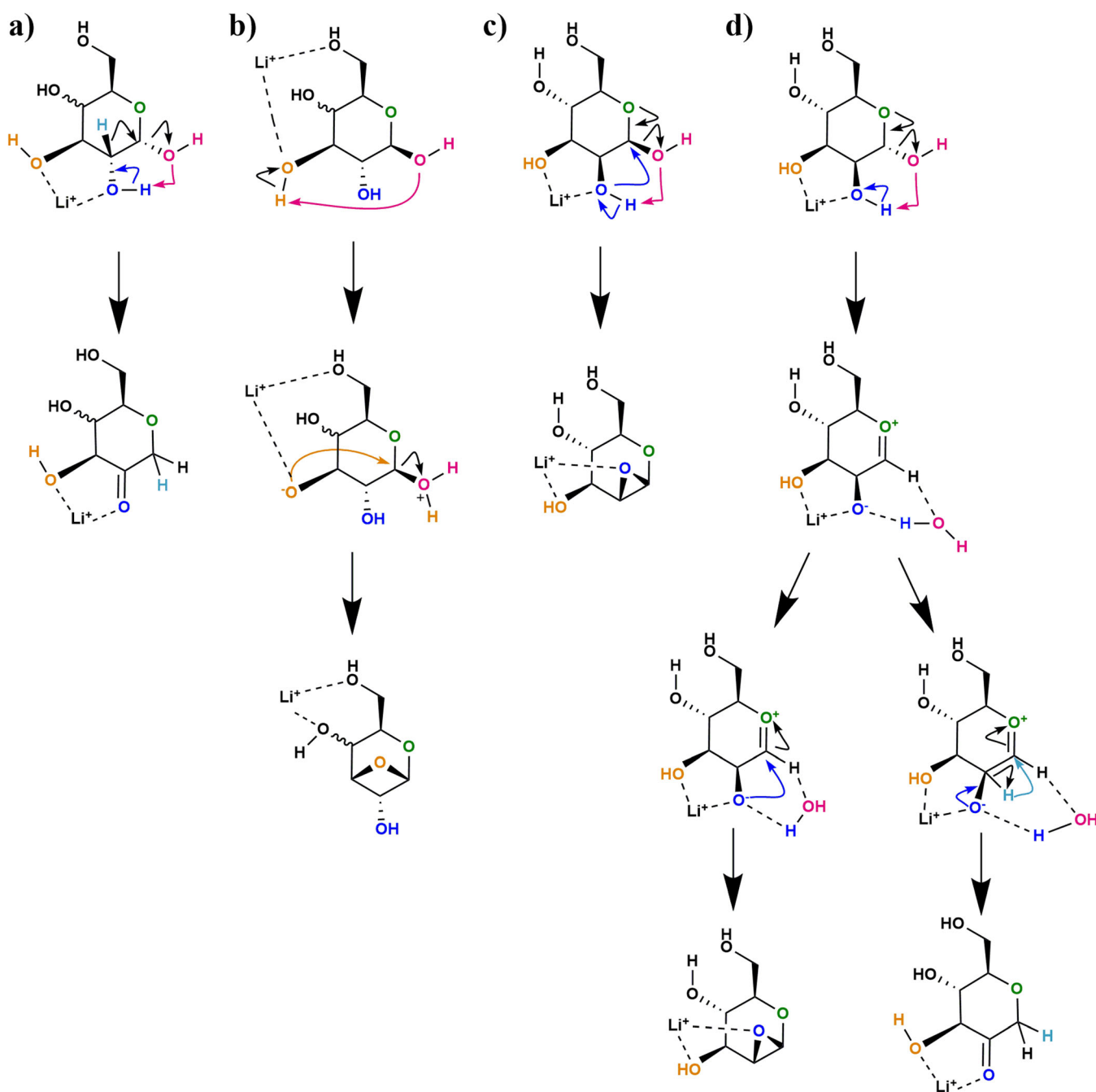
Scheme 1. Predicted, lowest energy mechanisms for water loss (B_1 ion formation) from the anomeric center of lithiated monosaccharides: (**a**) α-glucose and α-galactose anomers, (**b**) β-glucose and β-galactose anomers, (**c**) β-mannose anomer, and (**d**) α-mannose anomer

accompanied by concerted transfer of the C_α-H of C2 to the anomeric center (C1) and cleavage of the glycosidic bond. The net result is formation of a ketone at C2 (B_1 ion structures) and loss of water. Formation of the lithiated ketone B_1 ion structures from [α-glucose+Li]$^+$ and [α-galactose+Li]$^+$ requires at least 206 or 205 kJ mol^{-1} through an entropically favorable rate-limiting TS (Figure 4, Tables S4 and S5). [α-Mannose+Li]$^+$, in contrast, proceeds through a zwitterionic oxacarbenium TS and intermediate (Scheme 1d, Figure 4c). The rate-determining TS for the

lowest energy lithiated 1,2-anhydromannose B_1 ion formation reaction from [α-mannose+Li]$^+$ is substantially more energetically demanding (≥ 234 kJ mol^{-1}, Figure 4c, Table S6). This reaction initially forms a zwitterionic species in which an oxacarbenium functionality is adjacent to the Li$^+$ coordinated hydroxide at carbon 2 (Scheme 1d). Nucleophilic attack of hydroxide into the electropositive carbon 1 then forms the 1,2-anhydromannose B_1 ion as the water molecule departs. The alternate 1,2-H shift ketone-forming reaction is *initially* blocked for [α-
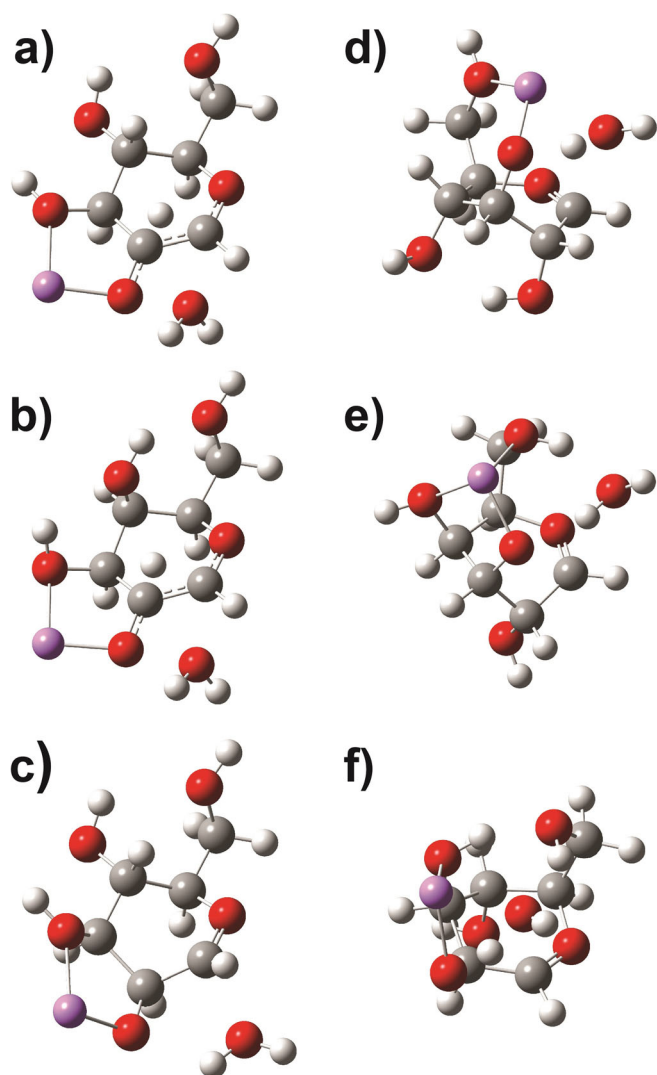
Figure 4. Transition state structures for water loss from (**a**) [α-glucose+Li]$^+$, (**b**) [α-galactose+Li]$^+$, and (**c**) [α-mannose+Li]$^+$, (**d**) [β-glucose+Li]$^+$, (**e**) [β-galactose+Li]$^+$, and (**f**) [β-mannose+Li]$^+$

mannose+Li]$^+$ by the change in stereochemistry at carbon 2 relative to α-glucose and α-galactose. Consequently, a ketone product is not *directly* formable. However, it is

possible to form the ketone B$_1$ ion from the dimer generated after cleavage of the anomeric C1–OH$_2^+$ bond (Scheme 1d, Figure S8). In the dimer, the non-covalently bound water molecule contains the hydroxyl group formerly at the anomeric center. The barrier to the ketone-forming 1,2-H shift reaction within the dimer is lower (227 kJ mol^{-1}, Table S6, Figure S8) than the preceding C1–OH$_2^+$ bond cleavage barrier and is entropically favorable (44 J K^{-1} mol^{-1}). Thus, provided the water molecule is not expelled immediately following C1–OH$_2^+$ bond cleavage, the ketone isomer is likely to be competitive. Similar types of rearrangements in post-cleavage dimers have been reported for peptides [53–57].

The β-anomers of lithiated glucose and galactose show distinct water loss pathways from the α-forms. These reactions are initiated from skew structures which facilitate nucleophilic attack by O3 into C1 with concerted transfer of the C3 hydroxyl proton to the anomeric oxygen as the glycosidic bond is cleaved (Scheme 1, Figure 4d, e). Lithiated 1,3-anhydroglucose and 1,3-anhydrogalactose B$_1$ ions are thus generated through comparatively low-energy, but entropically poor, hindered [58–61] transition structures (Tables 1 and 2; Figure 4d, e). These mechanisms are similar to those described previously by Chen et al. for sodiated glucose [35]. We note that production of a 1,4-anhydrogalactose B$_1$ ion might be expected from lithiated galactose. This possibility was tested but our calculations predict a higher energy barrier. In contrast, the [β-mannose+Li]$^+$ precursors are predicted to expel water from the anomeric center following proton transfer from the C2 hydroxyl group again producing a lithiated 1,2-anhydromannose B$_1$ ion in the process (Figure 4, Scheme 1c). The lowest energy form of this reaction requires at least 195 kJ mol^{-1} and is sterically hindered ($\Delta S_{298K} = -4.4$ J K^{-1} mol^{-1}, Table 3). An additional two, energetically more demanding ($\sim$ 6–15 kJ mol^{-1}), but entropically more favorable TSs of this type were also located. These structures will become increasingly more competitive as the gas phase in population becomes more energized [1, 58–62].

Our lowest energy calculated transition structures for both the α- and β-glucose analytes differ from those previously proposed [34]. We also located those transition structures [34], as well as many others not highlighted here (including

Table 1. Relative Energies of the Minima, Transition Structures, and Separated Products of Lithiated Glucose (β-D-Glucopyranosyl) Calculated at the M06-2X/6-31+G (d,p) Level of Theory. GM Is the Global Minimum of Potential Energy Surface of [β-D-Glucopyranosyl+Li]$^+$

Structures	E_{el}/H	E_{el+ZPE}/H	$\Delta E_{el+ZPE,0K}$/kJ mol^{-1}	ΔH_{298}/kJ mol^{-1}	ΔG_{298}/kJ mol^{-1}	ΔS_{298}/J K^{-1} mol^{-1}
GM	− 694.353897	− 694.353897	0	0	0	0
H$_2$O-loss TS	− 694.271475	− 694.071808	203.5	203.3	202.9	1.6
Ring opening	− 694.264314	− 694.065942	218.9	219.4	216.4	10.0
^{0,2}A$_1$ formation TS	− 694.275278	− 694.078204	186.7	189.1	181.0	27.5
1,2-H Shift TS	− 694.267432	− 694.070725	206.3	208.0	199.7	28.2
^{0,3}A$_1$ formation TS	− 694.280600	− 694.080930	179.6	182.6	172.6	34.3
[1,3-Anhydroglucose+Li]$^+$ B$_1$ + H$_2$O	− 694.287213	− 694.089555	156.9	162.2	113.7	165.4
1,3-Anhydroglucose + H$_2$O$\cdots$Li$^+$	− 694.242298	− 694.043536	277.7	281.5	228.4	181.1
^{0,2}A$_1$ + C$_2$H$_4$O$_2$	− 694.284397	− 694.088092	160.7	167.3	100.2	228.6
C$_4$H$_8$O$_4$ + ^{0,2}X$_0$	− 694.224246	− 694.030379	312.3	321.9	241.9	272.7
^{0,3}A$_1$ + C$_3$H$_6$O$_3$	− 694.280697	− 694.085066	168.7	174.9	106.4	2333.3
C$_3$H$_6$O$_3$ + ^{0,3}X$_0$	− 694.263866	− 694.068367	212.5	219.8	147.9	245.2

Table 2. Relative Energies of the Minima, Transition Structures, and Separated Products of Lithiated Galactose (β-D-Galactopyranosyl) Calculated at the M06-2X/6-31+G(d,p) Level of Theory. GM Is the Global Minimum of Potential Energy Surface of [β-D-Galactopyranosyl+Li]$^+$

Structures	E_{el}/H	E_{el+ZPE}/H	$\Delta E_{el+ZPE,0K}$/kJ mol^{-1}	ΔH_{298}/kJ mol^{-1}	ΔG_{298}/kJ mol^{-1}	ΔS_{298}/J K^{-1} mol^{-1}
GM	−694.357878	−694.153378	0	0	0	0
H$_2$O-loss TS	−694.281041	−694.080074	192.5	192.6	193.0	−1.6
Ring opening	−694.266263	−694.067332	225.9	225.7	224.9	2.8
^{0,2}A$_1$ formation TS	−694.273891	−694.076471	201.9	204.4	197.4	23.6
1,2-H Shift TS	−694.284436	−694.086410	175.8	177.9	172.6	18.1
^{0,3}A$_1$ formation TS	−694.288076	−694.089261	168.3	171.6	159.7	41.0
[1,3-Anhydrogalactose+Li]$^+$ B$_1$ + H$_2$O	−694.303411	−694.105085	126.8	131.3	84.7	158.8
1,3-Anhydrogalactose + H$_2$O···Li$^+$	−694.245041	−694.045950	282.1	285.4	233.0	178.6
^{0,2}A$_1$ + C$_2$H$_4$O$_2$	−694.275405	−694.079861	193.0	200.1	131.6	233.6
C$_4$H$_8$O$_4$ + ^{0,2}X$_0$	−694.234402	−694.039973	297.7	306.4	229.8	260.9
^{0,3}A$_1$ + C$_3$H$_6$O$_3$	−694.266605	−694.070993	216.3	223.7	151.8	245.0
C$_3$H$_6$O$_3$ + ^{0,3}X$_0$	−694.261718	−694.065941	229.6	237.8	164.4	250.0

non-anomeric oxygen losses), but these are less competitive (higher relative energies) based on our data.

## Cross-Ring Bond Cleavage Transition Structures: the A_n–X_m Pathways

Experimentally, all three analytes form both ^{0,2}A$_1$ and ^{0,3}A$_1$ ions but with differing onsets and propensities. Our calculations indicate that the mechanisms of formation of the ^{0,2}A$_1$ ion for lithiated glucose and galactose are similar to those previously proposed for larger systems [1–3] (Scheme 2). The ring opening occurs simultaneously to proton transfer from the anomeric hydroxyl group to the ring oxygen to form an aldehyde at C1 and a hydroxyl group at C5 from the hemiacetal groups (Scheme 2, Scheme S2). The barriers to ring opening vary with both anomeric configuration and specific monosaccharide. For example, the α-glucose and α-galactose congeners have lower barriers to ring opening than the β-forms, whereas for [mannose+Li]$^+$, this situation is reversed (Figure 5, Tables 1, 2, and 3, Tables S4–S6). Similarly, unlike the larger sodiated systems investigated previously by our group [1, 2], the rate-determining step for ^{0,2}A$_1$ ion formation is not universally the ring-opening TS. This again varies with both anomeric configuration and specific monosaccharide (Figure 5, Tables 1,

2, and 3, and Tables S4–S6). The second, potentially rate-limiting barrier to ^{0,2}A$_1$ ion formation is cleavage of the bond between C2 and C3. Concerted expulsion of 1,2-ethene-diol occurs along with the carbon-carbon bond cleavage and proton transfers (Scheme 2, Scheme S2, Figure S9 and S10), consistent with both the current (Figure S2, Tables S1–S3) and earlier labeling data [1–3, 33–35]. For the [mannose+Li]$^+$ forms, both the rate-determining TSs require more energy to populate than the glucose forms, consistent with the lower initial abundance of cross-ring cleavage peaks for these analytes (Figure 2c). Additionally, the [mannose+Li]$^+$ forms can expel either a cis or a trans 1,2-ethene-diol with similar barriers (210–214 kJ mol^{-1}), whereas the other hexoses eliminate the cis form preferentially (Table 3, Table S6, Figure S11).

Formation of the ^{0,3}A$_1$ ions is also predicted to begin with ring opening at the hemiacetal (Scheme 3, Figure 6). Direct loss of C$_3$H$_6$O$_3$ from this structure is energetically unfavorable, so instead a further isomerization reaction occurs prior to cleavage of the bond between C3 and C4. The isomerization involves an energetically demanding 1,2-H shift by the C$_\alpha$-H of C2 to C1 (Figure 6). The anomeric oxygen simultaneously abstracts a proton from the C2 hydroxyl group to leave a ketone at C2. The resulting isomer is the direct precursor for ^{0,3}A$_1$ ion generation. The final covalent bond cleavage stage of

Table 3. Relative Energies of the Minima, Transition Structures, and Separated Products of Lithiated Mannose (β-D-Mannopyranosyl) Calculated at the M06-2X/6-31+G(d,p) Level of Theory. GM Is the Global Minimum of Potential Energy Surface of β-D-Mannopyranosyl

Structures	E_{el}/H	E_{el+ZPE}/H	$\Delta E_{el+ZPE,0K}$/kJ mol^{-1}	ΔH_{298}/kJ mol^{-1}	ΔG_{298}/kJ mol^{-1}	ΔS_{298}/J K^{-1} mol^{-1}
GM	−694.359138	−694.154887	0	0	0	0
H$_2$O-loss TS	−694.277544	−694.080619	195.0	194.0	195.2	−4.4
Ring opening	−694.278757	−694.079472	198.0	197.3	195.9	5.0
^{0,2}A$_1$ formation TS (cis)	−694.274155	−694.074717	210.5	212.9	202.7	34.5
^{0,2}A$_1$ formation TS (trans)	−694.270687	−694.073253	214.3	217.4	207.0	35.4
1,2-H Shift TS	−694.267432	−694.070725	221.0	222.4	214.7	26.4
^{0,3}A$_1$ formation TS	−694.280600	−694.080930	194.2	197.0	187.5	32.5
H$_2$O + B$_1$: [1,2-anhydromannose+Li]$^+$	−694.280303	−694.082869	189.1	194.2	145.7	165.5
1,2-Anhydromannose + H$_2$O···Li$^+$	−694.273406	−694.073396	214.0	216.1	168.0	164.1
^{0,2}A$_1$ + C$_2$H$_4$O$_2$	−694.284397	−694.088094	175.4	181.7	115.1	226.8
C$_4$H$_8$O$_4$ + ^{0,2}X$_0$	−694.259796	−694.063957	238.7	245.5	175.8	237.5
^{0,3}A$_1$ + C$_3$H$_6$O$_3$	−694.280697	−694.085066	183.3	189.3	121.4	231.5
C$_3$H$_6$O$_3$ + ^{0,3}X$_0$	−694.263866	−694.068367	227.2	234.3	162.8	234.4
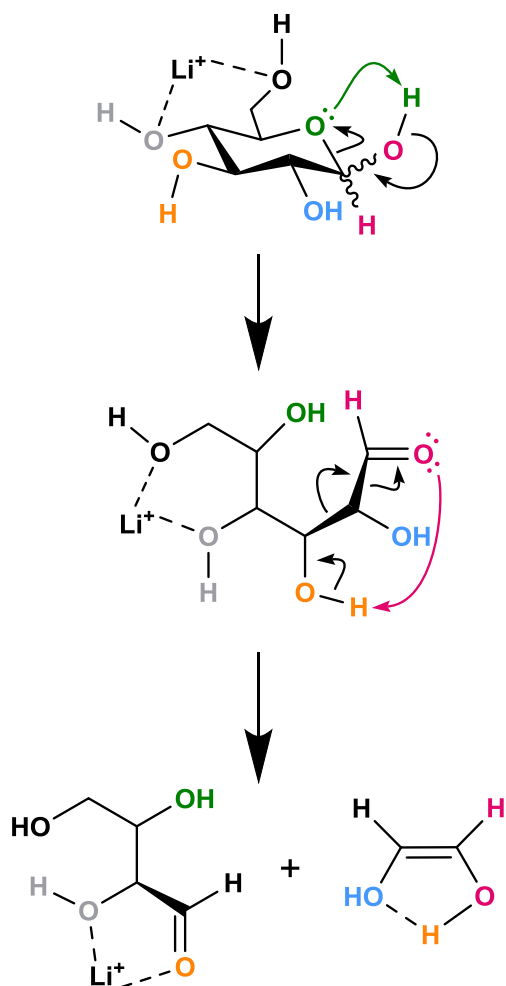
Scheme 2. Mechanism for ring opening followed by $^{0,2}A_1$ ion formation illustrated for lithiated glucose

this reaction then involves a complex concerted reaction. Transfer of two hydroxyl protons and concerted carbon-carbon bond cleavage (retro-aldol reaction [3]) results in generation of a lithium-bound dimer consisting of 2,3-dihydroxypropanal and (Z)-prop-1-ene-1,2,3-triol. Despite the dimer partners being isomers ($C_3H_6O_3$), our calculations predict that the 2,3-dihydroxypropanal will dominantly retain the Li^+ in agreement with lithium affinity calculations, thereby producing the $^{0,3}A_1$ peak. This agrees with the loss of $C_3H_3D_3O_3$ (HC(OD)=C(OD)–H2COD, Figure S2, Scheme S3) in our deuterated hydroxyl labeling experiments and the other regiospecific labeling data (Tables S1–S3). For larger sodiated systems, the analogous highly strained 1,2-H shift was found to be the rate-limiting step to $^{0,3}A_2$ formation [2]. For the lithiated monosaccharides discussed here, this is not uniformly the case. This makes broad statements governing all analyte forms difficult. However, for all lithiated analytes, the ring-open products are entropically favored over the pyranose ring forms. Consequently, these reactions will be increasingly facile once ring opening has been achieved. In most cases, the ring-opening TS is rate limiting enthalpically. Furthermore, even in those cases in which a slightly higher barrier exists
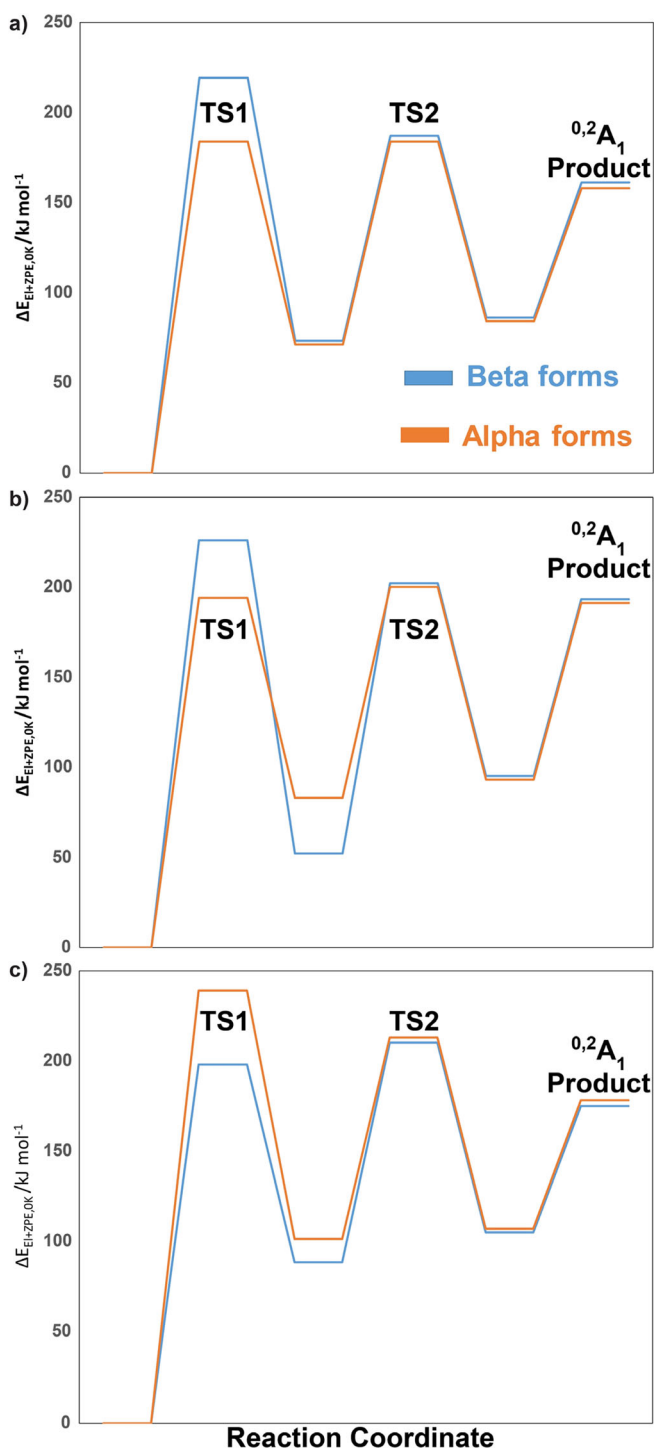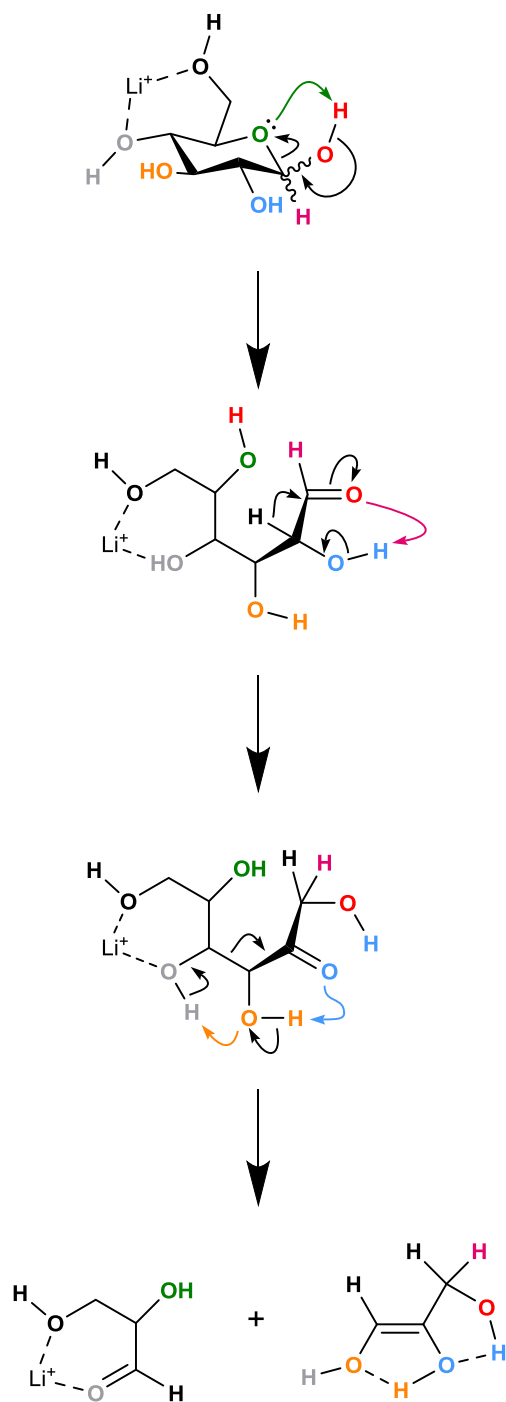

Figure 5. Summarized energetics for $^{0,2}A_1$ ion formation: (**a**) [glucose+Li]$^+$, (**b**) [galactose+Li]$^+$, and (**c**) [mannose+Li]$^+$. TS1 = ring opening; TS2 = C2–C3 bond cleavage

after ring opening along the reaction coordinate, the relatively low ΔS_{298K} of the ring-opening TS likely limits [2, 58, 61, 62] the progress of the reaction. Once ring opening is complete and sufficient energy is available for subsequent degradation, the branching ratio between the $^{0,3}A_1$ and $^{0,2}A_1$ peaks is a function of the relative entropic favorability of these two

Scheme 3. Mechanism for ring opening followed by 1,2-H transfer then $^{0,3}A_1$ ion formation illustrated for lithiated glucose

processes (and indirectly the stability of the A_1 ion products) so ΔG_{298K} is the pertinent measure of the reaction favorability.

Conclusions

There are broad similarities in the fragmentation chemistry of lithiated glucose, galactose, and mannose, but also structural differences. There are also differences based on anomeric configuration. For example, while all analytes expel a water
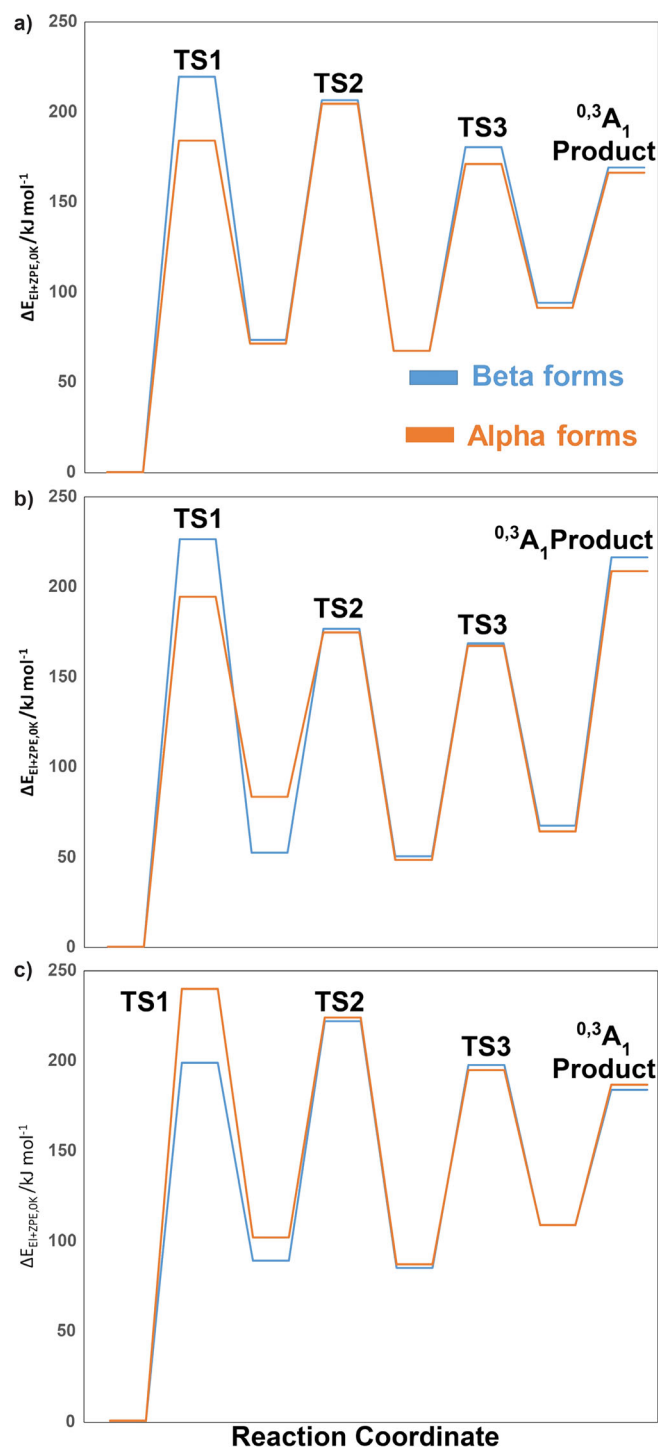

Figure 6. Summarized energetics for $^{0,3}A_1$ ion formation: (**a**) [glucose+Li]$^+$, (**b**) [galactose+Li]$^+$, and (**c**) [mannose+Li]$^+$. TS1 = ring opening; TS2 = 1,2-H transfer; TS3 = C3–C4 bond cleavage

molecule from the anomeric center at low collision energies, the product ion structure differs between the α- and β-forms for glucose and galactose (lithiated C2 ketones from the α-forms vs. 1,3-anhydrohexose isomers from the β-forms). The dissociation chemistry of both mannose forms is significantly affected by the hydroxyl stereochemistry at carbon 2, which

results in production of lithiated 1,2-anhydromannose from both precursor types. Additionally, provided water loss is not instantaneous, the α-anomer can also isomerize to generate a ketone structure at C2 through a concerted 1,2-migration of the of the C2-H to C1. The resulting product is indistinguishable to that formed from [α-glucose+Li]$^{+}$. All analytes investigated form both $^{0,3}A_1$ and $^{0,2}A_1$ ions in mechanisms substantially (though not necessarily solely) limited by the entropically relatively poor ring-opening transition structures. The lowest energy A_1 ion-forming mechanisms are consistent with those advocated previously in the literature [2, 3, 33] and our own labeling data.

Acknowledgments

References

1. Bythell, B.J., Abutokaikah, M.T., Wagoner, A.R., Guan, S., Rabus, J.M.: Cationized carbohydrate gas-phase fragmentation chemistry. J. Am. Soc. Mass Spectrom. **28**, 688–703 (2017)

2. Rabus, J.M., Abutokaikah, M.T., Ross, R.T., Bythell, B.J.: Sodium-cationized carbohydrate gas-phase fragmentation chemistry: influence of glycosidic linkage position. Phys. Chem. Chem. Phys. **19**, 25643–25652 (2017)

3. Hofmeister, G.E., Zhou, Z., Leary, J.A.: Linkage position determination in lithium-cationized disaccharides: tandem mass spectrometry and semi-empirical calculations. J. Am. Chem. Soc. **113**, 5964–5970 (1991)

4. An, H.J., Kronewitter, S.R., de Leoz, M.L.A., Lebrilla, C.B.: Glycomics and disease markers. Curr. Opin. Chem. Biol. **13**, 601–607 (2009)

5. Bertozzi, C.R., Sasisekharan, R.: Glycomics. In: Varki, A., Cummings, R.D., Esko, J.D., Freeze, H.H., Stanley, P., Bertozzi, C.R., Hart, G.W., Etzler, M.E. (eds.) Essentials of Glycobiology. Cold Spring Harbor Laboratory Press, Cold Spring Harbor (2009)

6. Huang, Y., Dodds, E.D.: Discrimination of isomeric carbohydrates as the electron transfer products of group II cation adducts by ion mobility spectrometry and tandem mass spectrometry. Anal. Chem. **87**, 5664–5668 (2015)

7. Hoffmann, W., Hofmann, J., Pagel, K.: Energy-resolved ion mobility-mass spectrometry—a concept to improve the separation of isomeric carbohydrates. J. Am. Soc. Mass Spectrom. **25**, 471–479 (2014)

8. Zhu, F., Glover, M.S., Shi, H., Trinidad, J.C., Clemmer, D.E.: Populations of metal-glycan structures influence MS fragmentation patterns. J. Am. Soc. Mass Spectrom. **26**, 25–35 (2015)

9. Zhu, M., Bendiak, B., Clowers, B., Hill, H.H.: Ion mobility separation of isomeric carbohydrate precursor ions and acquisition of their independent tandem mass spectra. Anal. Bioanal. Chem. **394**, 1853–1867 (2009)

10. Pagel, K., Harvey, D.J.: Ion mobility–mass spectrometry of complex carbohydrates: collision cross sections of sodiated N-linked glycans. Anal. Chem. **85**, 5138–5145 (2013)

11. Struwe, W.B., Baldauf, C., Hofmann, J., Rudd, P.M., Pagel, K.: Ion mobility separation of deprotonated oligosaccharide isomers—evidence for gas-phase charge migration. Chem. Commun. **52**, 12353–12356 (2016)

12. Gray, C.J., Schindler, B., Migas, L.G., Pičmanová, M., Allouche, A.R., Green, A.P., Mandal, S., Motawia, M.S., Sánchez-Pérez, R., Bjarnholt, N., Møller, B.L., Rijs, A.M., Barran, P.E., Compagnon, I., Eyers, C.E., Flitsch, S.L.: Bottom-up elucidation of glycosidic bond stereochemistry. Anal. Chem. **89**, 4540–4549 (2017)

13. Gray, C.J., Thomas, B., Upton, R., Migas, L.G., Eyers, C.E., Barran, P.E., Flitsch, S.L.: Applications of ion mobility mass spectrometry for high throughput, high resolution glycan analysis. Biochim. Biophys. Acta BBA - Gen. Subj. **1860**, 1688–1709 (2016)

14. Morrison, K.A., Clowers, B.H.: Contemporary glycomic approaches using ion mobility–mass spectrometry. Curr. Opin. Chem. Biol. **42**, 119–129 (2018)

15. Kailemia, M.J., Ruhaak, L.R., Lebrilla, C.B., Amster, I.J.: Oligosaccharide analysis by mass spectrometry: a review of recent developments. Anal. Chem. **86**, 196–212 (2014)

16. Reinhold, V.N., Reinhold, B.B., Costello, C.E.: Carbohydrate molecular weight profiling, sequence, linkage, and branching data: ES-MS and CID. Anal. Chem. **67**, 1772–1784 (1995)

17. Zaia, J.: Mass spectrometry of oligosaccharides. Mass Spectrom. Rev. **23**, 161–227 (2004)

18. Ashline, D.J., Lapadula, A.J., Liu, Y.-H., Lin, M., Grace, M., Pramanik, B., Reinhold, V.N.: Carbohydrate structural isomers analyzed by sequential mass spectrometry. Anal. Chem. **79**, 3830–3842 (2007)

19. Morrison, K.A., Bendiak, B.K., Clowers, B.H.: Enhanced mixture separations of metal adducted tetrasaccharides using frequency encoded ion mobility separations and tandem mass spectrometry. J. Am. Soc. Mass Spectrom. **28**, 664–677 (2017)

20. Cancilla, M.T., Penn, S.G., Carroll, J.A., Lebrilla, C.B.: Coordination of alkali metals to oligosaccharides dictates fragmentation behavior in matrix assisted laser desorption ionization/Fourier transform mass spectrometry. J. Am. Chem. Soc. **118**, 6736–6745 (1996)

21. Huang, Y., Pu, Y., Yu, X., Costello, C.E., Lin, C.: Mechanistic study on electronic excitation dissociation of the cellobiose-Na+ complex. J. Am. Soc. Mass Spectrom. **27**, 319–328 (2016)

22. Campbell, M.T., Chen, D., Glish, G.L.: Distinguishing linkage position and anomeric configuration of glucose–glucose disaccharides by water adduction to lithiated molecules. Anal. Chem. **90**, 2048–2054 (2018)

23. Konda, C., Londry, F., Bendiak, B., Xia, Y.: Assignment of the stereochemistry and anomeric configuration of sugars within oligosaccharides via overlapping disaccharide ladders using MSn. J. Am. Soc. Mass Spectrom. **25**, 1441–1450 (2014)

24. Brown, D.J., Stefan, S.E., Berden, G., Steill, J.D., Oomens, J., Eyler, J.R., Bendiak, B.: Direct evidence for the ring opening of monosaccharide anions in the gas phase: photodissociation of aldohexoses and aldohexoses derived from disaccharides using variable-wavelength infrared irradiation in the carbonyl stretch region. Carbohydr. Res. **346**, 2469–2481 (2011)

25. Spengler, B., Dolce, J.W., Cotter, R.J.: Infrared laser desorption mass spectrometry of oligosaccharides: fragmentation mechanisms and isomer analysis. Anal. Chem. **62**, 1731–1737 (1990)

26. Harvey, D.J., Bateman, R.H., Green, M.R.: High-energy collision-induced fragmentation of complex oligosaccharides ionized by matrix-assisted laser desorption/ionization mass spectrometry. J. Mass Spectrom. **32**, 167–187 (1997)

27. Hernandez, O., Isenberg, S., Steinmetz, V., Glish, G.L., Maitre, P.: Probing mobility-selected saccharide isomers: selective ion–molecule reactions and wavelength-specific IR activation. J. Phys. Chem. A. **119**, 6057–6064 (2015)

28. Eike, M., Isabel, G. .F.A., Mateusz, M., Thomas Daniel, A., Waldemar, H., Struwe Weston, B., Hahm Heung, S., Sandy, G., Wieland, S., Seeberger Peter, H., von Gert, H., Kevin, P.: Glycan fingerprinting via cold-ion infrared spectroscopy. Angew. Chem. Int. Ed. **56**, 11248–11251 (2017)

29. Masellis, C., Khanal, N., Kamrath, M.Z., Clemmer, D.E., Rizzo, T.R.: Cryogenic vibrational spectroscopy provides unique fingerprints for glycan identification. J. Am. Soc. Mass Spectrom. **28**, 2217–2222 (2017)

30. Campbell, M.T., Chen, D., Wallbillich, N.J., Glish, G.L.: Distinguishing biologically relevant hexoses by water adduction to the lithium-cationized molecule. Anal. Chem. **89**, 10504–10510 (2017)

31. Laine, R.A.: Invited commentary: A calculation of all possible oligosaccharide isomers both branched and linear yields 1.05 × 1012 structures for a reducing hexasaccharide: the isomer barrier to development of single-method saccharide sequencing or synthesis systems. Glycobiology. **4**, 759–767 (1994)

32. Asam, M.R., Ray, K.L., Glish, G.L.: Collision-induced signal enhancement: a method to increase product ion intensities in MS/MS and MSn experiments. Anal. Chem. **70**, 1831–1837 (1998)

33. Jiang, W., Wysocki, V.H., Dodds, E.D., Miesfeld, R.L., Scaraffia, P.Y.: Differentiation and quantification of C1 and C2 13C-labeled glucose by tandem mass spectrometry. Anal. Biochem. **404**, 40–44 (2010)

34. Tsai, S.-T., Chen, J.-L., Ni, C.-K.: Does low-energy collision-induced dissociation of lithiated and sodiated carbohydrates always occur at anomeric carbon of the reducing end? Rapid Commun. Mass Spectrom. **31**, 1835–1844 (2017)

35. Chen, J.-L., Nguan, H.S., Hsu, P.-J., Tsai, S.-T., Liew, C.Y., Kuo, J.-L., Hu, W.-P., Ni, C.-K.: Collision-induced dissociation of sodiated glucose and identification of anomeric configuration. Phys. Chem. Chem. Phys. **19**, 15454–15462 (2017)

36. Tan, Y., Zhao, N., Liu, J., Li, P., Stedwell, C.N., Yu, L., Polfer, N.C.: Vibrational signatures of isomeric lithiated N-acetyl-D-hexosamines by gas-phase infrared multiple-photon dissociation (IRMPD) spectroscopy. J. Am. Soc. Mass Spectrom. **28**, 539–550 (2017)

37. Schnupf, U., Willett, J.L., Bosma, W.B., Momany, F.A.: DFT study of α- and β-d-allopyranose at the B3LYP/6-311++G** level of theory. Carbohydr. Res. **342**, 196–216 (2007)

38. Appell, M., Willett, J.L., Momany, F.A.: DFT study of α- and β-d-mannopyranose at the B3LYP/6-311++G** level. Carbohydr. Res. **340**, 459–468 (2005)

39. Marianski, M., Supady, A., Ingram, T., Schneider, M., Baldauf, C.: Assessing the accuracy of across-the-scale methods for predicting carbohydrate conformational energies for the examples of glucose and α-maltose. J. Chem. Theory Comput. **12**, 6157–6168 (2016)

40. Supady, A., Blum, V., Baldauf, C.: First-principles molecular structure search with a genetic algorithm. J. Chem. Inf. Model. **55**, 2338–2348 (2015)

41. Frisch, M.J., Trucks, G.W., Schlegel, H.B., Scuseria, G.E., Robb, M.A., Cheeseman, J.R., Scalmani, G., Barone, V., Mennucci, B., Petersson, G.A., Nakatsuji, H., Caricato, M., Li, X., Hratchian, H.P., Izmaylov, A.F., Bloino, J., Zheng, G., Sonnenberg, J.L., Hada, M., Ehara, M., Toyota, K., Fukuda, R., Hasegawa, J., Ishida, M., Nakajima, T., Honda, Y., Kitao, O., Nakai, H., Vreven, T., Montgomery, J.A., Peralta, J.E., Ogliaro, F., Bearpark, M., Heyd, J.J., Brothers, E., Kudin, K.N., Staroverov, V.N., Kobayashi, R., Normand, J., Raghavachari, K., Rendell, A., Burant, J.C., Iyengar, S.S., Tomasi, J., Cossi, M., Rega, N., Millam, J.M., Klene, M., Knox, J.E., Cross, J.B., Bakken, V., Adamo, C., Jaramillo, J., Gomperts, R., Stratmann, R.E., Yazyev, O., Austin, A.J., Cammi, R., Pomelli, C., Ochterski, J.W., Martin, R.L., Morokuma, K., Zakrzewski, V.G., Voth, G.A., Salvador, P., Dannenberg, J.J., Dapprich, S., Daniels, A.D., Farkas, Foresman, J.B., Ortiz, J.V., Cioslowski, J., Fox, D.J.: Gaussian 09, Revision E.01. Gaussian, Inc., Wallingford (2009)

42. Zhao, Y., Schultz, N.E., Truhlar, D.G.: Exchange-correlation functional with broad accuracy for metallic and nonmetallic compounds, kinetics, and noncovalent interactions. J. Chem. Phys. **123**(16), 161103 (2005)

43. Zhao, Y., Truhlar, D.G.: The M06 suite of density functionals for main group thermochemistry, thermochemical kinetics, noncovalent interactions, excited states, and transition elements: two new functionals and systematic testing of four M06-class functionals and 12 other functionals. Theor. Chem. Accounts. **120**, 215–241 (2008)

44. Halgren, T.A.: Merck molecular force field. I. Basis, form, scope, parameterization, and performance of MMFF94. J. Comput. Chem. **17**, 490–519 (1996)

45. Halgren, T.A.: Merck molecular force field. II. MMFF94 van der Waals and electrostatic parameters for intermolecular interactions. J. Comput. Chem. **17**, 520–552 (1996)

46. Halgren, T.A.: Merck molecular force field. III. Molecular geometries and vibrational frequencies for MMFF94. J. Comput. Chem. **17**, 553–586 (1996)

47. Halgren, T.A., Nachbar, R.B.: Merck molecular force field. IV. Conformational energies and geometries for MMFF94. J. Comput. Chem. **17**, 587–615 (1996)

48. Halgren, T.A.: Merck molecular force field. V. Extension of MMFF94 using experimental data, additional computational data, and empirical rules. J. Comput. Chem. **17**, 616–641 (1996)

49. Domon, B., Costello, C.E.: A systematic nomenclature for carbohydrate fragmentations in FAB-MS/MS spectra of glycoconjugates. Glycoconj. J. **5**, 397–409 (1988)

50. Firdoussi, A.E., Lafitte, M., Tortajada, J., Kone, O., Salpin, J.-Y.: Characterization of the glycosidic linkage of underivatized disaccharides by interaction with Pb2+ ions. J. Mass Spectrom. **42**, 999–1011 (2007)

51. Boutreau, L., Léon, E., Salpin, J.-Y., Amekraz, B., Moulin, C., Tortajada, J.: Gas-phase reactivity of silver and copper coordinated monosaccharide cations studied by electrospray ionization and tandem mass spectrometry. Eur. J. Mass Spectrom. **9**, 377–390 (2003)

52. IUPAC: Conformational nomenclature for five and six-membered ring forms of monosaccharides and their derivatives. Eur. J. Biochem. **111**, 295–298 (1980)

53. Bleiholder, C., Osburn, S., Williams, T.D., Suhai, S., Van Stipdonk, M., Harrison, A.G., Paizs, B.: Sequence-scrambling fragmentation pathways of protonated peptides. J. Am. Chem. Soc. **130**, 17774–17789 (2008)

54. Erlekam, U., Bythell, B.J., Scuderi, D., Van Stipdonk, M., Paizs, B., Maître, P.: Infrared spectroscopy of fragments of protonated peptides: direct evidence for macrocyclic structures of b5 ions. J. Am. Chem. Soc. **131**, 11503–11508 (2009)

55. Chen, X., Yu, L., Steill, J.D., Oomens, J., Polfer, N.C.: Effect of peptide fragment size on the propensity of cyclization in collision-induced dissociation: oligoglycine b(2)-b(8). J. Am. Chem. Soc. **131**, 18272–18282 (2009)

56. Tang, X.J., Thibault, P., Boyd, R.K.: Fragmentation reactions of multiply-protonated peptides and implications for sequencing by tandem mass spectrometry with low-energy collision-induced dissociation. Anal. Chem. **65**, 2824–2834 (1993)

57. Bythell, B.J., Knapp-Mohammady, M., Paizs, B., Harrison, A.G.: Effect of the His residue on the cyclization of b ions. J. Am. Soc. Mass Spectrom. **21**, 1352–1363 (2010)

58. Rodgers, M.T., Armentrout, P.B.: Cationic noncovalent interactions: energetics and periodic trends. Chem. Rev. **116**, 5642–5687 (2016)

59. Wu, R.R., Rodgers, M.T.: O2 protonation controls threshold behavior for N-glycosidic bond cleavage of protonated cytosine nucleosides. J. Phys. Chem. B. **120**, 4803–4811 (2016)

60. Carl, D.R., Chatterjee, B.K., Armentrout, P.B.: Threshold collision-induced dissociation of Sr2+(H2O)x complexes (x=1–6): an experimental and theoretical investigation of the complete inner shell hydration energies of Sr2+. J. Chem. Phys. **132**, 044303 (2010)

61. Heaton, A.L., Armentrout, P.B.D.: Thermodynamics and mechanism of the deamidation of sodium-bound asparagine. J. Am. Chem. Soc. **130**, 10227–10232 (2008)

62. Abutokaikah, M.T., Guan, S., Bythell, B.J.: Stereochemical sequence ion selectivity: proline versus pipecolic-acid-containing protonated peptides. J. Am. Soc. Mass Spectrom. **28**, 182–189 (2017)